Supporting Information

In vivo two-photon microscopy reveals the contribution of Sox9$^+$ cell to kidney regeneration in a mouse model with extracellular vesicle treatment

Supplemental Table 1. Primers used in the qPCR assay.

Gene	Forward primer sequence, 5'-3'	Reverse primer sequence, 5'-3'
Bax	CATGTTTGCTGATGGCAACT	TGATCAGCTCGGGCACTTTA
Bad	GAGTGAGCAGGAAGACGCTA	CCCTGCTGATGAATGTTGCT
Fas	TTGCTGGCTCACAGTTAAGA	TTCAGGTTGGCATGGTTGAC
Fasl	GGTCAGTTTTTCCCTGTCCA	AATCCCATTCCAACCAGAGC
Casp3	AGAGAGACATTCATGGGCCT	AGTTTCGGCTTTCCAGTCAG
Casp9	AATGGGACTCACAGCAAAGG	CTCAAGTTTGTCACGGTCCA
Fn1	CAAATCGTGCAGCCTCAATC	GGAATCTTTAGGGCGCTCAT
Col1a1	CCAATGGTGAGACGTGGAA	GTCCCTCGACTCCTACATCT
Tgfb1	ACAATTCCTGGCGTTACCTT	CCCTGTATTCCGTCTCCTTG
Gapdh	TGACCACAGTCCATGCCATC	CAGGTCAGGTCCACCACTGA

Shown is the sequences of primers in 5'-3' orientation for real-time qPCR used in this study.

Supplemental experimental procedures

Cells

The MSCs used in this study were isolated from human placenta tissue (hP-MSCs) as previously described(1,2). The hP-MSCs used in subsequent experiments were between passages 4 to 10, which were cultured in EV-free medium (Dulbecco's modified Eagle's medium (DMEM)/F12 medium (Gibco, Grand Island, NY) with 10% EV-free fetal bovine serum (FBS; HyClone, Logan, UT) and 100 U/mL penicillin−streptomycin (Gibco)). The EV-free FBS was obtained by ultracentrifugation at 100,000g for 18 hours at 1:4 dilution(3). Human kidney proximal tubule cells (HK2) were purchased from ATCC (ATCC, Manassas, VA) and maintained in keratinocyte serum free medium (K-SFM) (Gibco) with the following components: 0.05 mg/mL bovine pituitary extract (BPE), 5 ng/mL human recombinant epidermal growth factor (EGF), and 100 units/mL penicillin−streptomycin. All these cells were negative from mycoplasma tests and were maintained in a humidified incubator with 5% CO_2 at 37 °C.

EVs isolation and characterization

In this study, EVs were purified from the supernatant of hP-MSCs as previously described(4). In brief, hP-MSCs were continuous passage cultured every two days with EV-free medium. The cell culture supernatant was collected during the subcultivation. The supernatant was centrifuged at 500 g for 10 min to remove any cell contaminations, followed by a centrifugation step of 10,000 g for 30 min to discard cell debris and apoptotic bodies. Then, EVs were isolated by ultracentrifugation at 100,000 g for 70 min. Finally, the EVs were washed by Dulbecco's

phosphate-buffered saline (DPBS) and pelleted again via a second ultracentrifugation at 100,000 g for 2 h. All the above procedures were performed at 4 °C. Total protein amount of the final EVs pellets was measured by a Bicinchoninic Acid (BCA) Protein Assay Kit (Thermo Scientific, Madison, WI).

The transmission electron microscopy (TEM; Talos F200C, Hillsboro, OR) was used to verify the morphology of EVs. A drop of EVs (1 μg/μL) was loaded in a carbon film (Zhongjingkeji Technology, Beijing, China) with the following negative staining by 2% phosphotungstic acid. Then, the air-dried samples were ready for capturing of TEM images (magnification 30.0k). The protein markers (CD9 and Alix) and the negative protein composition (GM130) of EVs were analyzed by the western blot assay. The particle size and number of EVs were determined by nanoparticle tracking analysis (NTA) (NanoSight NS300, Malvern Panalytical, Malvern, UK).

Bioluminescent imaging of Gluc-labeled EVs

The EVs used in BLI were labeled by Gaussia luciferase (Gluc) as previously described(5). In brief, the lentivirus carried the gene sequences of the recombinant human lactadherin fused with Gluc (Gluc-lac) were transduced into hP-MSCs. The transduced hP-MSCs stably expressed the Gluc-lac fusion protein, which was a membrane-associated protein mainly found in EVs. Then, the supernatant of the transduced hP-MSCs was harvested to separate the Gluc-labeled EVs by ultracentrifugation. For the intravital imaging, the mice which were implanted with abdominal imaging windows were subjected to unilateral (left) renal IRI. Then the mice

received three consecutive intravenous injections of Gluc-labeled EVs at a dose of 100 μg in a volume of 100 μL. At the indicated time points, the mice were imaged immediately using the IVIS Lumina Imaging System after intraperitoneal injection of the substrate of Gluc, water-soluble coelenterazine (5 mg/kg; Nanolight Technology, Pinetop, AZ).

RNA extraction and real-time quantitative PCR analysis

The total RNAs of kidney tissues were isolated by TRIzol reagent (Invitrogen, Grand Island, NY) following the manufacturer's protocol. Then, 2 μg total RNAs were reverse transcribed using BioScript All-in-One cDNA Synthesis SuperMix (Bimake, Houston, TX). Real-time quantitative polymerase chain reaction (qPCR) was conducted in the CFX96 Touch System (Bio-Rad, Hercules, CA) machine by using qPCR SYBR green master mix (Yeasen, Shanghai, China). Relative gene expression was normalized to *Gapdh* and analyzed with the $2^{-\Delta\Delta Ct}$ method. The sequences of primers used in this study are shown in **Table S1**.

Protein extraction and western blotting analysis

The cells and EVs prepared for western blotting were lysed in radio immunoprecipitation assay (RIPA) buffer (Solarbio, Shanghai, China) and the total protein was quantified using a BCA Protein Assay Kit (Thermo Scientific). The total proteins were diluted into 4× SDS-PAGE loading buffer and boiled for 10 min. Then, samples were electrophoresed on 10% polyacrylamide gels and transferred to 0.2 μm polyvinylidene fluoride (PVDF) membranes (Millipore, Darmstadt, Germany). After blocking with 5% nonfat milk for 2 h, the PVDF membranes were incubated with primary antibodies overnight at 4 °C, and then for 2 h at room

temperature with secondary antibodies. Antibodies used include anti-CD9 (1:2000; Abcam, Cambridge, UK), anti-Alix (1:1000; Wanleibio, Shengyang, China), anti-GM130 (1:2000; Abcam), anti-Sox9 (1:2000; Cell Signaling Technology, Beverly, MA), and anti-actin (1:5000; CWBIO, Beijing, China). The blots were imaged by using a Tanon-5200 Chemiluminescence Imaging System (Tanon Science & Technology Co Ltd., Shanghai, China).

References

1. Tao, H., Chen, X., Cao, H., Zheng, L., Li, Q., Zhang, K., Han, Z., Han, Z.-C., Guo, Z., Li, Z., and Wang, L. (2019) Mesenchymal stem cell-derived extracellular vesicles for corneal wound repair. *Stem Cells Int* **2019**, 5738510.
2. Liang, L., Li, Z., Ma, T., Han, Z., Du, W., Geng, J., Jia, H., Zhao, M., Wang, J., Zhang, B., Feng, J., Zhao, L., Rupin, A., Wang, Y., and Han, Z. C. (2017) Transplantation of human placenta-derived mesenchymal stem cells alleviates critical limb ischemia in diabetic nude rats. *Cell Transplant* **26**, 45-61
3. Thery, C., Witwer, K. W., Aikawa, E., Alcaraz, M. J., Anderson, J. D., Andriantsitohaina, R., Antoniou, A., Arab, T., Archer, F., Atkin-Smith, G. K., Ayre, D. C., Bach, J. M., Bachurski, D., Baharvand, H., Balaj, L., Baldacchino, S., Bauer, N. N., Baxter, A. A., Bebawy, M., Beckham, C., Bedina Zavec, A., Benmoussa, A., Berardi, A. C., Bergese, P., Bielska, E., Blenkiron, C., Bobis-Wozowicz, S., Boilard, E., Boireau, W., Bongiovanni, A., Borras, F. E., Bosch, S., Boulanger, C. M., Breakefield, X., Breglio, A. M., Brennan, M. A., Brigstock, D. R., Brisson, A., Broekman, M. L., Bromberg, J. F., Bryl-Gorecka, P., Buch, S., Buck, A. H., Burger, D., Busatto, S., Buschmann, D., Bussolati, B., Buzas, E. I., Byrd, J. B., Camussi, G., Carter, D. R., Caruso, S., Chamley, L. W., Chang, Y. T., Chen, C., Chen, S., Cheng, L., Chin, A. R., Clayton, A., Clerici, S. P., Cocks, A., Cocucci, E., Coffey, R. J., Cordeiro-da-Silva, A., Couch, Y., Coumans, F. A., Coyle, B., Crescitelli, R., Criado, M. F., D'Souza-Schorey, C., Das, S., Datta Chaudhuri, A., de Candia, P., De Santana, E. F., De Wever, O., Del Portillo, H. A.,

Demaret, T., Deville, S., Devitt, A., Dhondt, B., Di Vizio, D., Dieterich, L. C., Dolo, V., Dominguez Rubio, A. P., Dominici, M., Dourado, M. R., Driedonks, T. A., Duarte, F. V., Duncan, H. M., Eichenberger, R. M., Ekstrom, K., El Andaloussi, S., Elie-Caille, C., Erdbrugger, U., Falcon-Perez, J. M., Fatima, F., Fish, J. E., Flores-Bellver, M., Forsonits, A., Frelet-Barrand, A., Fricke, F., Fuhrmann, G., Gabrielsson, S., Gamez-Valero, A., Gardiner, C., Gartner, K., Gaudin, R., Gho, Y. S., Giebel, B., Gilbert, C., Gimona, M., Giusti, I., Goberdhan, D. C., Gorgens, A., Gorski, S. M., Greening, D. W., Gross, J. C., Gualerzi, A., Gupta, G. N., Gustafson, D., Handberg, A., Haraszti, R. A., Harrison, P., Hegyesi, H., Hendrix, A., Hill, A. F., Hochberg, F. H., Hoffmann, K. F., Holder, B., Holthofer, H., Hosseinkhani, B., Hu, G., Huang, Y., Huber, V., Hunt, S., Ibrahim, A. G., Ikezu, T., Inal, J. M., Isin, M., Ivanova, A., Jackson, H. K., Jacobsen, S., Jay, S. M., Jayachandran, M., Jenster, G., Jiang, L., Johnson, S. M., Jones, J. C., Jong, A., Jovanovic-Talisman, T., Jung, S., Kalluri, R., Kano, S. I., Kaur, S., Kawamura, Y., Keller, E. T., Khamari, D., Khomyakova, E., Khvorova, A., Kierulf, P., Kim, K. P., Kislinger, T., Klingeborn, M., Klinke, D. J., 2nd, Kornek, M., Kosanovic, M. M., Kovacs, A. F., Kramer-Albers, E. M., Krasemann, S., Krause, M., Kurochkin, I. V., Kusuma, G. D., Kuypers, S., Laitinen, S., Langevin, S. M., Languino, L. R., Lannigan, J., Lasser, C., Laurent, L. C., Lavieu, G., Lazaro-Ibanez, E., Le Lay, S., Lee, M. S., Lee, Y. X. F., Lemos, D. S., Lenassi, M., Leszczynska, A., Li, I. T., Liao, K., Libregts, S. F., Ligeti, E., Lim, R., Lim, S. K., Line, A., Linnemannstons, K., Llorente, A., Lombard, C. A., Lorenowicz, M. J., Lorincz, A. M., Lotvall, J., Lovett, J., Lowry, M. C., Loyer, X., Lu, Q., Lukomska, B., Lunavat, T. R., Maas, S. L., Malhi, H., Marcilla, A., Mariani, J., Mariscal, J., Martens-Uzunova, E. S., Martin-Jaular, L., Martinez, M. C., Martins, V. R., Mathieu, M., Mathivanan, S., Maugeri, M., McGinnis, L. K., McVey, M. J., Meckes, D. G., Jr., Meehan, K. L., Mertens, I., Minciacchi, V. R., Moller, A., Moller Jorgensen, M., Morales-Kastresana, A., Morhayim, J., Mullier, F., Muraca, M., Musante, L., Mussack, V., Muth, D. C., Myburgh, K. H., Najrana, T., Nawaz, M., Nazarenko, I., Nejsum, P., Neri, C., Neri, T., Nieuwland, R., Nimrichter, L., Nolan, J. P., Nolte-'t Hoen, E. N., Noren Hooten, N., O'Driscoll, L., O'Grady, T., O'Loghlen, A., Ochiya, T., Olivier, M., Ortiz, A., Ortiz, L. A., Osteikoetxea, X., Ostergaard, O., Ostrowski, M., Park, J.,

Pegtel, D. M., Peinado, H., Perut, F., Pfaffl, M. W., Phinney, D. G., Pieters, B. C., Pink, R. C., Pisetsky, D. S., Pogge von Strandmann, E., Polakovicova, I., Poon, I. K., Powell, B. H., Prada, I., Pulliam, L., Quesenberry, P., Radeghieri, A., Raffai, R. L., Raimondo, S., Rak, J., Ramirez, M. I., Raposo, G., Rayyan, M. S., Regev-Rudzki, N., Ricklefs, F. L., Robbins, P. D., Roberts, D. D., Rodrigues, S. C., Rohde, E., Rome, S., Rouschop, K. M., Rughetti, A., Russell, A. E., Saa, P., Sahoo, S., Salas-Huenuleo, E., Sanchez, C., Saugstad, J. A., Saul, M. J., Schiffelers, R. M., Schneider, R., Schoyen, T. H., Scott, A., Shahaj, E., Sharma, S., Shatnyeva, O., Shekari, F., Shelke, G. V., Shetty, A. K., Shiba, K., Siljander, P. R., Silva, A. M., Skowronek, A., Snyder, O. L., 2nd, Soares, R. P., Sodar, B. W., Soekmadji, C., Sotillo, J., Stahl, P. D., Stoorvogel, W., Stott, S. L., Strasser, E. F., Swift, S., Tahara, H., Tewari, M., Timms, K., Tiwari, S., Tixeira, R., Tkach, M., Toh, W. S., Tomasini, R., Torrecilhas, A. C., Tosar, J. P., Toxavidis, V., Urbanelli, L., Vader, P., van Balkom, B. W., van der Grein, S. G., Van Deun, J., van Herwijnen, M. J., Van Keuren-Jensen, K., van Niel, G., van Royen, M. E., van Wijnen, A. J., Vasconcelos, M. H., Vechetti, I. J., Jr., Veit, T. D., Vella, L. J., Velot, E., Verweij, F. J., Vestad, B., Vinas, J. L., Visnovitz, T., Vukman, K. V., Wahlgren, J., Watson, D. C., Wauben, M. H., Weaver, A., Webber, J. P., Weber, V., Wehman, A. M., Weiss, D. J., Welsh, J. A., Wendt, S., Wheelock, A. M., Wiener, Z., Witte, L., Wolfram, J., Xagorari, A., Xander, P., Xu, J., Yan, X., Yanez-Mo, M., Yin, H., Yuana, Y., Zappulli, V., Zarubova, J., Zekas, V., Zhang, J. Y., Zhao, Z., Zheng, L., Zheutlin, A. R., Zickler, A. M., Zimmermann, P., Zivkovic, A. M., Zocco, D., and Zuba-Surma, E. K. (2018) Minimal information for studies of extracellular vesicles 2018 (misev2018): A position statement of the international society for extracellular vesicles and update of the misev2014 guidelines. *J Extracell Vesicles* **7**, 1535750

4. Du, W., Zhang, K., Zhang, S., Wang, R., Nie, Y., Tao, H., Han, Z., Liang, L., Wang, D., Liu, J., Liu, N., Han, Z., Kong, D., Zhao, Q., and Li, Z. (2017) Enhanced proangiogenic potential of mesenchymal stem cell-derived exosomes stimulated by a nitric oxide releasing polymer. *Biomaterials* **133**, 70-81

5. Zhang, K., Zhao, X., Chen, X., Wei, Y., Du, W., Wang, Y., Liu, L., Zhao, W., Han, Z., Kong, D., Zhao, Q., Guo, Z., Han, Z., Liu, N., Ma, F., and Li, Z. (2018) Enhanced

therapeutic effects of mesenchymal stem cell-derived exosomes with an injectable hydrogel for hindlimb ischemia treatment. *ACS Appl Mater Interfaces* **10**, 30081-30091

Supplemental Figures & Legends

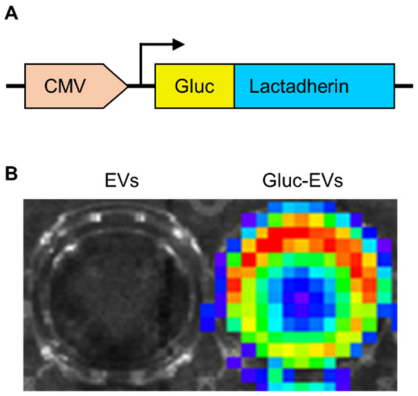

Figure S1. Gluc and DiI-labeled EVs imaging.

(A) The scheme of Gluc-lac fusion protein. (B) BLI analysis of Gluc-labeled EVs.

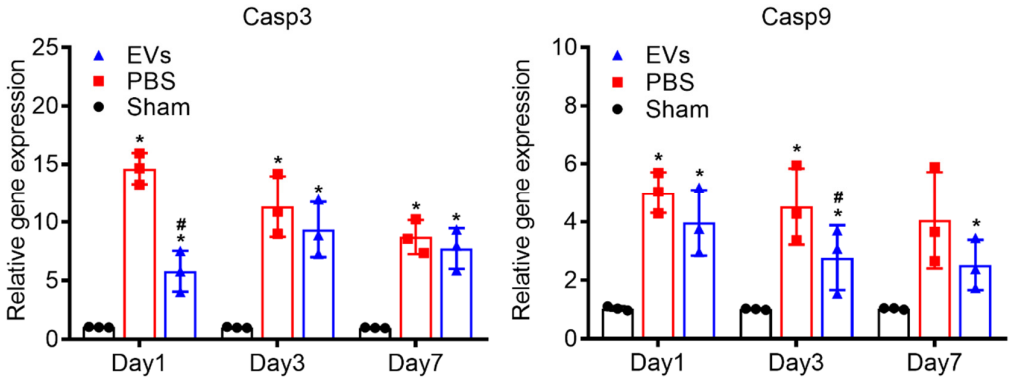

Figure S2. Apoptosis-related gene expression in injured kidneys.

Real-time qPCR analysis of apoptosis-related genes in kidneys on days 1, 3, and 7 after IRI. Relative gene expression was normalized to *Gapdh*. Data are expressed as scatter plots with mean ± standard deviation (SD). $^{*}P<0.05$ versus Sham; $^{\#}P<0.05$ versus PBS. All experiments were performed in triplicate.

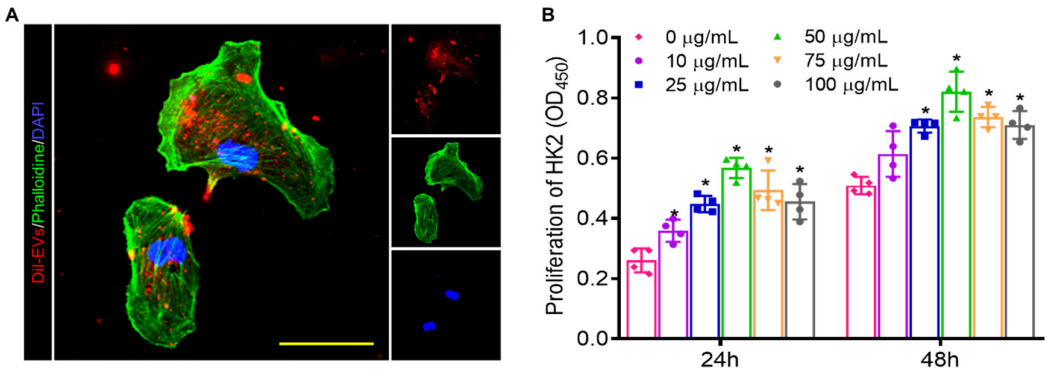

Figure S3. EVs promoted the proliferation of HK2 cells.

(A) The internalization of DiI-labeled EVs by HK2 cells. Scale bar, 20 μm. (B) Cell proliferation assay of HK2 cells administrated with EVs. Data are expressed as scatter plots with mean ± standard deviation (SD). $^{*}P<0.05$ versus 0 μg/mL.

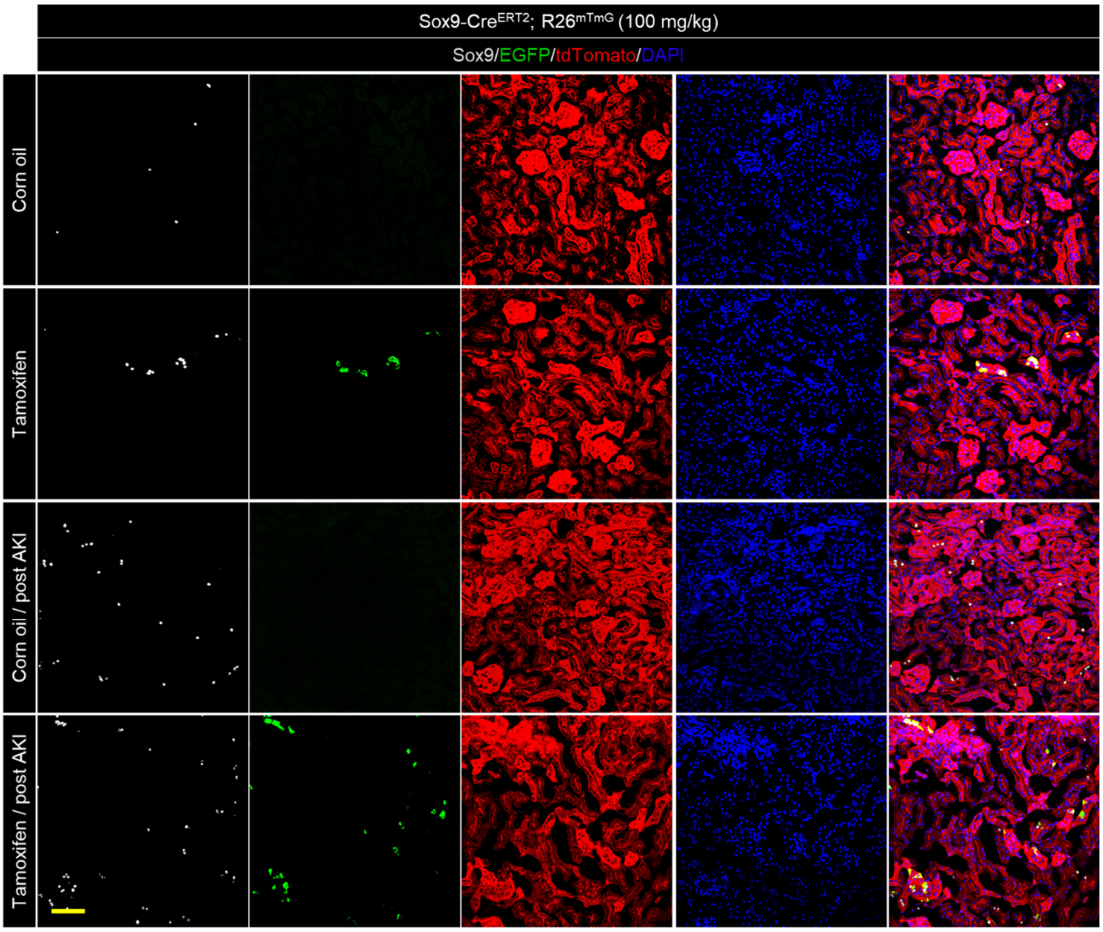

Figure S4. Validation and fidelity of the g genetic lineage tracing model.

Representative images for co-localization analysis of anti-Sox9 immunostaining (grey) and Sox9-Cre^{ERT2} activated EGFP fluorescence in kidneys after 3 times tamoxifen or corn oil injection before and post AKI. Scale bar, 50 μm.

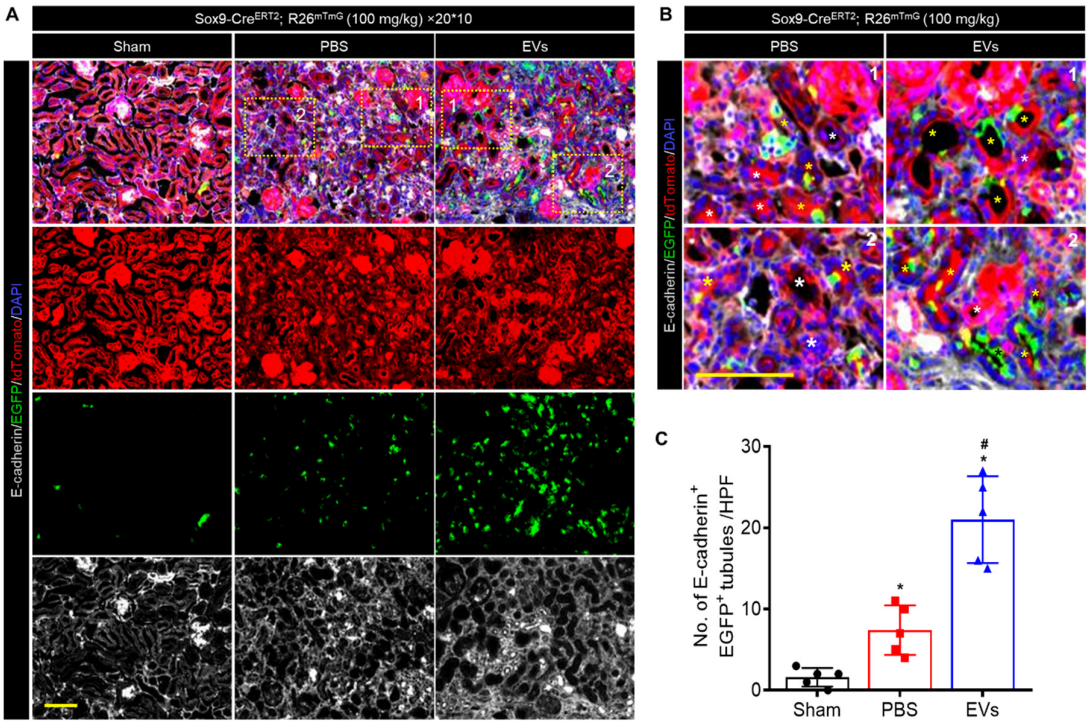

Figure S5. Anti-E-cadherin immunostaining of renal tissues from Sox9-Cre^{ERT2}; R26^{mTmG} mice.

(A) Representative images and (B) local zoom images for co-localization analysis of anti-E-cadherin immunostaining (grey) and Sox9-Cre^{ERT2} activated EGFP fluorescence in kidneys on day 14 post injury. Scale bar, 100 μm. (C) Quantification of E-cadherin^{+}/EGFP co-labeled tubules in the sections of figure 5B. Data are expressed as scatter plots with mean ± standard deviation (SD). $^{*}P<0.05$ versus Sham; $^{\#}P<0.05$ versus PBS.

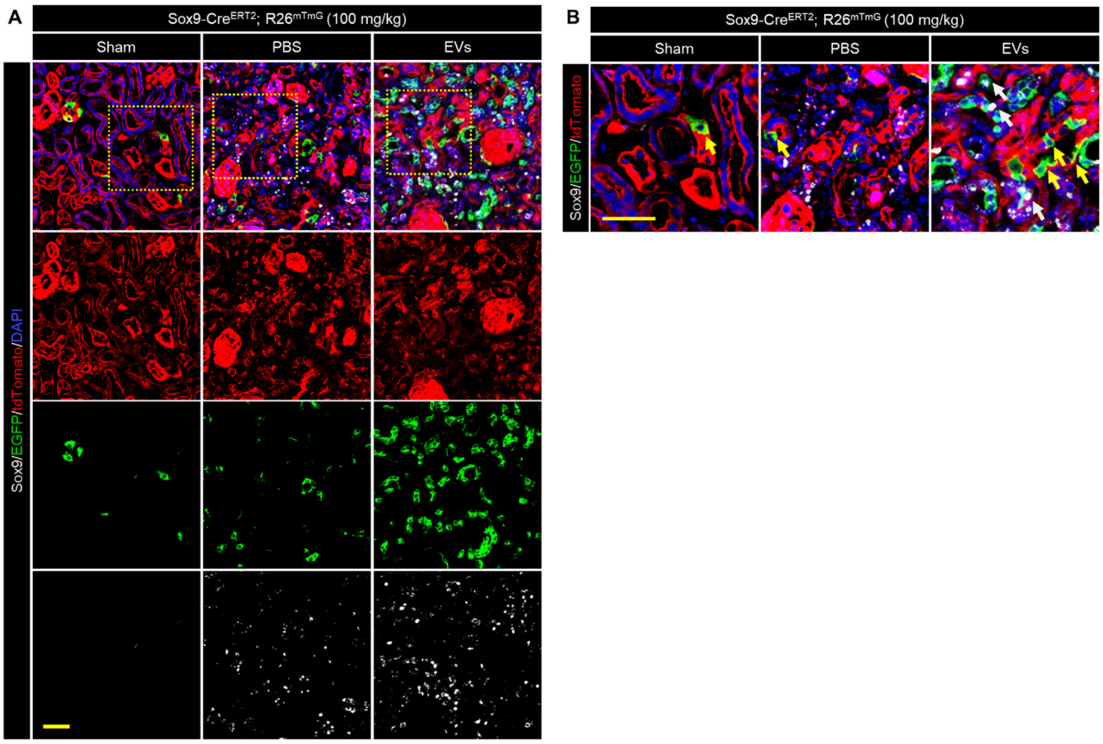

Figure S6. Anti-Sox9 immunostaining of renal tissues from Sox9-Cre^{ERT2}; R26^{mTmG} mice.

(A) Confocal images and (B) local zoom images for co-localization analysis of anti-Sox9 immunostaining (grey) and Sox9-Cre^{ERT2} activated EGFP fluorescence in kidneys on day 14 post IRI. White arrowheads highlighted Sox9^{+}/EGFP co-labeled cells, and yellow arrowheads highlighted the Sox9 negative but EGFP labeled cells. Scale bar, 50 μm.

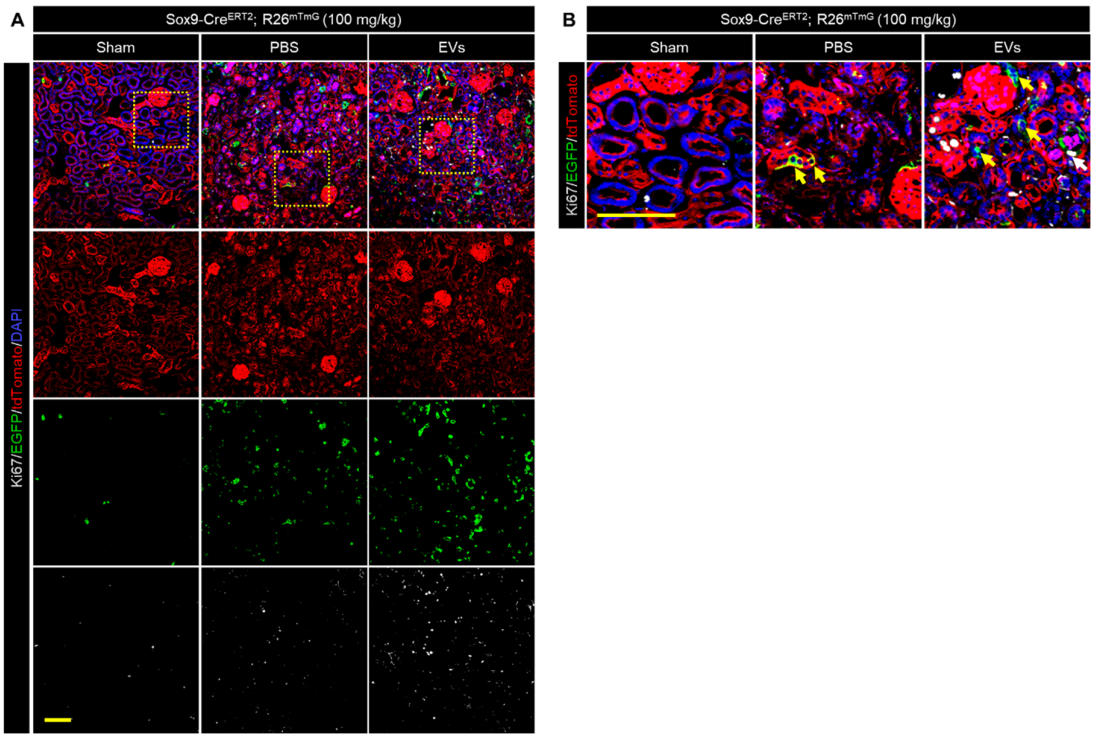

Figure S7. Anti-Ki67 immunostaining of renal tissues from Sox9-Cre^{ERT2}; R26^{mTmG} mice.

(A) Confocal images and (B) local zoom images for co-localization analysis of anti-Ki67 immunostaining (grey) and Sox9-Cre^{ERT2} activated EGFP fluorescence in kidneys on day 14 post injury. White arrowheads highlighted Ki67^{+}/EGFP co-labeled cells, and yellow arrowheads highlighted the Ki67^{-} but EGFP labeled cells. Scale bar, 100 μm.

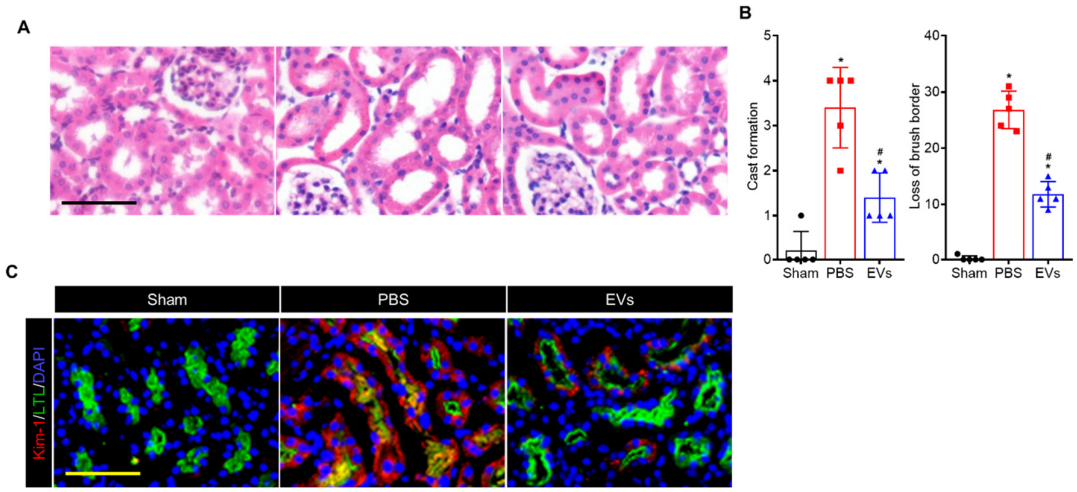

Figure S8. Histological analysis of injured kidneys.

(A) Representative images and local zoom images of Figure 7A in injured renal tissues. Scale bar, 100 μm. (B) Quantitative assessments of cast formation and injured tubules. Data are expressed as scatter plots with mean ± standard deviation (SD). $^{*}P<0.05$ versus Sham; $^{\#}P<0.05$ versus PBS. (C) Representative images and local zoom images of Figure 7A anti-Kim-1 immunostaining (red) on day 3 post IRI. The proximal tubules were co-stained by FITC-labeled LTL (green). Scale bar, 100 μm.

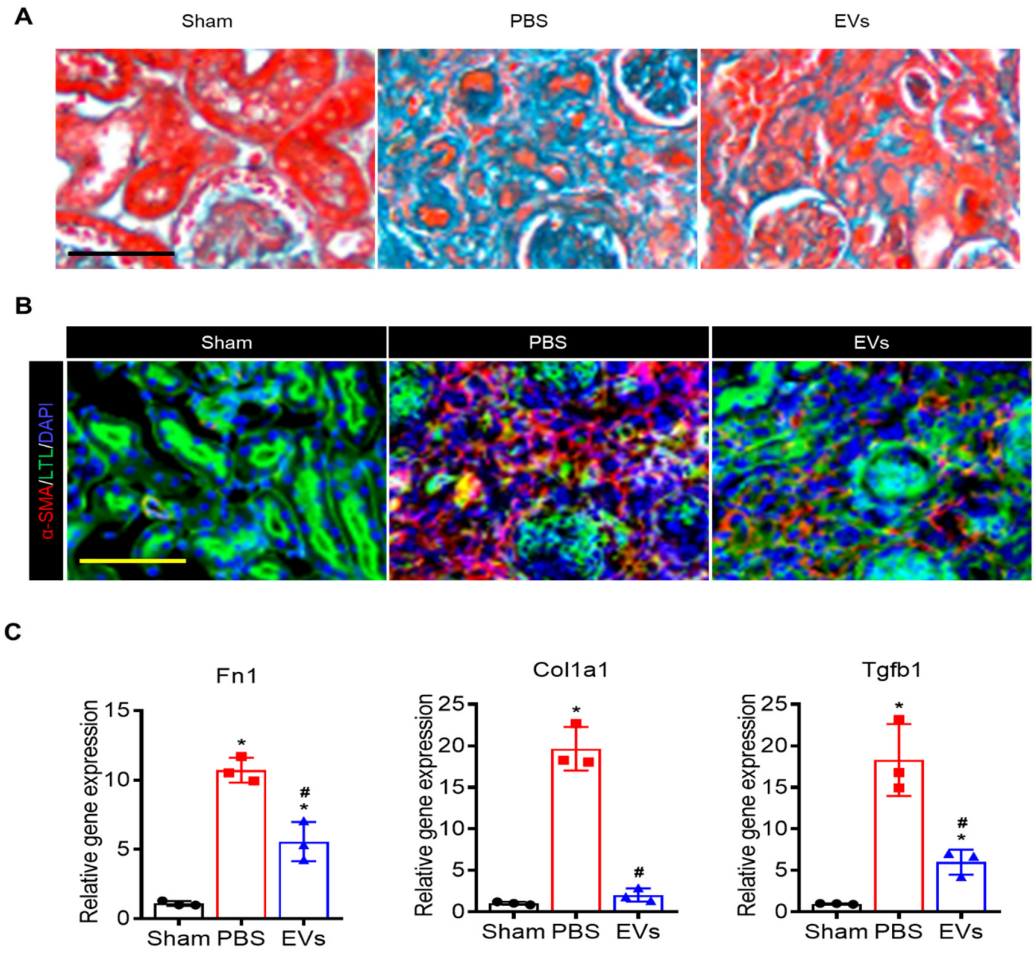

Figure S9. Fibrosis examination in injured kidneys.

(A) Representative images and local zoom images of Figure 7D Masson staining for renal tissues harvested on day 28 post IRI. Scale bar, 100 μm. (B) Representative images and local zoom images of Figure 7D anti-αSMA immunostaining (red) for renal tissues harvested on day 28 post IRI. The proximal tubules were co-stained by FITC-labeled LTL (green). Scale bar, 100 μm. (C) Real-time qPCR analysis of fibrosis-related genes in kidneys on day 28 after IRI. Relative gene expression was normalized to *Gapdh*. Data are expressed as scatter plots with mean ± standard deviation (SD). $^{*}P<0.05$ versus Sham; $^{\#}P<0.05$ versus PBS. All experiments were performed in triplicate.

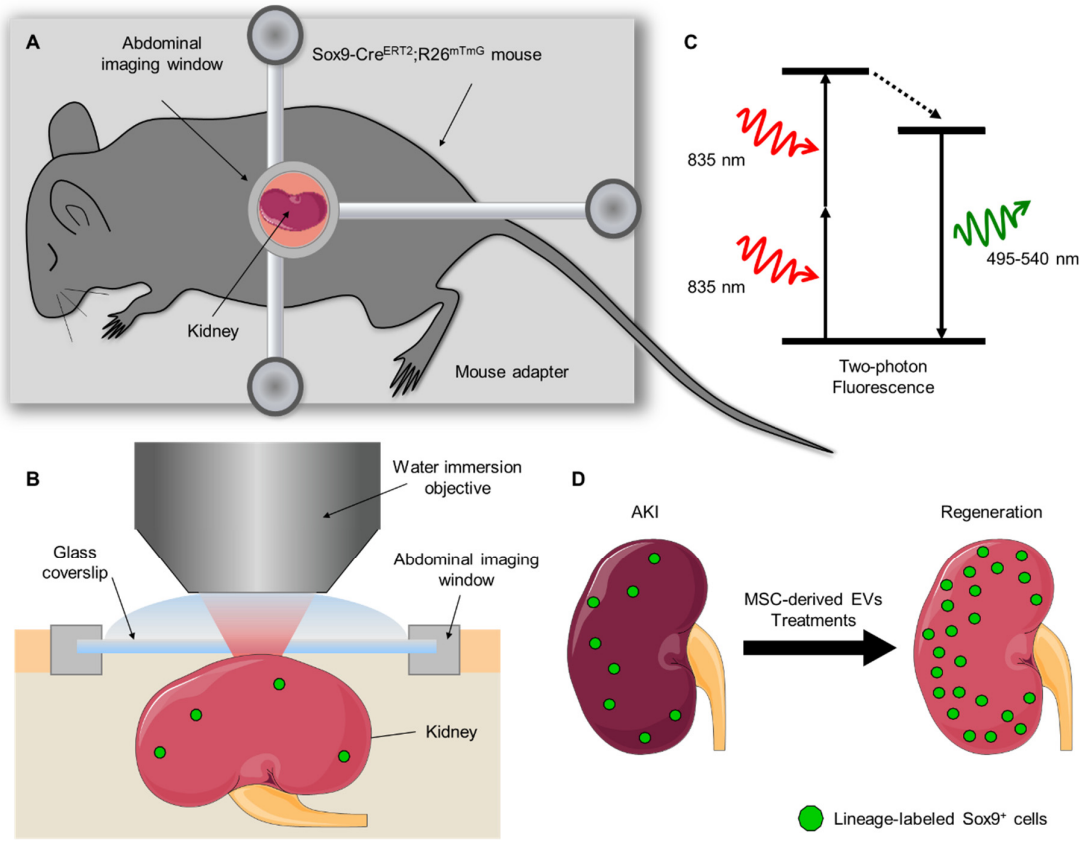

Figure S10. Schematic diagram of two-photon living imaging of Sox9 positive cells in living mouse.

(**A**) The Sox9-Cre^{ERT2}; R26^{mTmG} mouse was immobilized on a mouse adapter with AIW upwards. (**B**) Schematic of two-photon living imaging preparation of exposed cortex, with glass-sealed abdominal imaging window and microscope objective positioning. (**C**) Basic mechanism of two-photon fluorescence imaging. (**D**) EVs accelerated renal regeneration via activating the expansion of Sox9^{+} cells.

Video S1-S4. Video of 3D exhibition for the injured kidney in the same mouse treated with EVs.

The 3D exhibition of the renal structure in the same Sox9-Cre^{ERT2}; R26^{mTmG} mouse treated with EVs on day 1 (Video S1), day 3 (Video S2), day 7 (Video S3), and day 14 (Video S4) after IRI. All cells in Sox9-Cre^{ERT2}; R26^{mTmG} mouse expressed membrane-localized tdTomato. After the injection of tamoxifen, the Sox9 expressing cells and their descendants had membrane-localized EGFP fluorescence expression replacing the tdTomato fluorescence. The green highlighted spots in the kidney represented the renal tubules formed by the descendants of Sox9^{+} cells. The videos were captured by using a two-photon microscope and reconstructed by Volocity high-performance image analysis software.